DOI: 10.1002/chem.200701253

Carboxylate Ligands Drastically Enhance the Rates of Oxo Exchange and Hydrogen Peroxide Disproportionation by Oxo Manganese Compounds of Potential Biological Significance

Lionel Dubois,[b] Jacques Pécaut,[b] Marie-France Charlot,[c] Carole Baffert,[d] Marie-Noëlle Collomb,[d] Alain Deronzier,[d] and Jean-Marc Latour*[a]

Abstract: To mimic the carboxylate-rich active site of the manganese catalases more closely we introduced carboxylate groups into dimanganese complexes in place of nitrogen ligands. The series of dimanganese(III,IV) complexes of tripodal ligands $[Mn_2(L)_2(O)_2]^{3+/+/-/3-}$ was extended from those of tpa (**1**) and H(bpg) (**2**) to those of H_2(pda) (**3**) and H_3(nta) (**4**) (tpa = tris-picolylamine, H(bpg) = bis-picolylglycylamine, H_2(pda) = picolyldiglycylamine, H_3(nta) = nitrilotriacetic acid). While **3** $[Mn_2(pda)_2(O)_2][Na(H_2O)_3]$ could be synthesized at −20 °C and characterized in the solid state, **4** $[Mn_2(nta)_2(O)_2]^{3-}$ could be obtained and studied only in solution at −60 °C. A new synthetic procedure for the dimanganese(III,III) complexes was devised, using stoichiometric reduction of the dimanganese(III,IV) precursor by the benzil radical with EPR monitoring. This enabled the preparation of the parent dimanganese(III,III) complex **5** $[Mn_2(tpa)_2(O)_2](ClO_4)_2$, which was structurally characterized. The UV/visible, IR, EPR, magnetic, and electrochemical properties of complexes **1**–**3** and **5** were analyzed to assess the electronic changes brought about by the carboxylate replacement of pyridine ligands. The kinetics of the oxo ligand exchanges with labeled water was examined in acetonitrile solution. A dramatic effect of the number of carboxylates was evidenced. Interestingly, the influence of the second carboxylate substitution differs from that of the first one probably because this substitution occurs on an out-of-plane coordination while the former occurs in the plane of the $[Mn_2O_2]$ core. Indeed, on going from **1** to **3** the exchange rate was increased by a factor of 50. Addition of triethylamine caused a rate increase for **1**, but not for **3**. The abilities of **1**–**3** to disproportionate H_2O_2 were assessed volumetrically. The disproportionation exhibited a sensitivity corresponding to the carboxylate substitution. These observations strongly suggest that the carboxylate ligands in **2** and **3** act as internal bases.

Keywords: catalases · enzyme models · H_2O_2 disproportionation · manganese · oxo exchange

[a] Dr. J.-M. Latour
CEA-DSV, iRTSV, Laboratoire de Chimie et Biologie des Métaux/PMB
CEA-Grenoble, 38054 Grenoble (France)
Fax: (+33) 438-78-3462
E-mail: Jean-Marc.Latour@cea.fr

[b] Dr. L. Dubois, Dr. J. Pécaut
CEA-DSM, Laboratoire de Chimie Inorganique et Biologique
UMR E 3 CEA—UJF, CEA-Grenoble
38054 Grenoble (France)

[c] Dr. M.-F. Charlot
Laboratoire de Chimie Inorganique
Institut de Chimie Moléculaire et des Matériaux d'Orsay
UMR CNRS 8182, Univ Paris-Sud
91405 Orsay Cedex (France)

[d] Dr. C. Baffert, Dr. M.-N. Collomb, Dr. A. Deronzier
Département de Chimie Moléculaire, UMR CNRS 5250
ICMG FR-2607, Université Joseph Fourier Grenoble 1
B.P. 53, 38041 Grenoble Cedex 9 (France)

Supporting information for this article is available on the WWW under http://www.chemeurj.org/ or from the author.

Introduction

Although it is a by-product of aerobic respiration, hydrogen peroxide is considered highly deleterious because its reduction gives rise to the hydroxyl radical, which is able to attack all cell components. Therefore, as soon as it is produced, H_2O_2 is disproportionated by the catalase enzymes, which play a pivotal role in the protection of living cells against oxidative stress.[1,2] Most of these enzymes are hemoproteins, but manganese is a cofactor of a few of bacterial origin.[3–5]

Crystallographic studies have revealed that the active sites of the Mn catalases found in the bacteria *Thermus thermophilus*[6] and *Lactobacillus plantarum*[7] each comprise two manganese atoms triply bridged by the carboxylate group of a glutamate and two water-derived ligands. In the reduced state of the enzymes ($Mn^{II}Mn^{II}$), these two ligands are probably a hydroxide ion and a water molecule,[8] while in the oxidized state ($Mn^{III}Mn^{III}$)[9] they are oxide ions as in

the "superoxidized state" ($Mn^{III}Mn^{IV}$).[10] In addition, each manganese ion is bound to the protein chain through one histidine and one glutamate.

Biochemical studies[11] have shown that neither the $Mn^{III}Mn^{IV}$ nor the $Mn^{II}Mn^{III}$ states are functional, and elegant spectroscopic studies[12] have demonstrated that during catalysis the Mn pair shuttles between the oxidation states $Mn^{II}Mn^{II}$ and $Mn^{III}Mn^{III}$. So far, the fast kinetics of the enzymatic reaction ($k_{cat} \approx 10^5\ s^{-1}$)[13] and the fact that the oxidized and the reduced forms both react with the same substrate (H_2O_2) have precluded detailed mechanistic studies. As a consequence, most mechanistic hypotheses have been based on studies of biomimetic compounds.[14–16] Numerous reports on the "catalase-like reaction" have been published for very diverse manganese compounds. Nevertheless, the most detailed mechanistic studies were performed on complexes of binucleating ligands involving either alkoxides[17–19] or phenolates,[20–23] which stabilize the dimanganese unit by providing it with an internal bridge. Depending upon the Mn ligands, all oxidation states of the pair from $Mn^{II}Mn^{II}$ to $Mn^{IV}Mn^{IV}$ have been implicated in the catalysis. Conversely, few detailed studies have been performed with manganese complexes possessing a bis-(μ-oxo) bridging pattern, in spite of the fact that it is the one found in the enzymes.[9,10]

An examination of the literature shows that only a few bis-(μ-oxo)bis-manganese(III) complexes have been structurally characterized,[24–30] while their $Mn^{III}Mn^{IV}$ counterparts are plethoric.[14–16,31] In addition, all of these complexes possess hindered nitrogen ligands, and moreover no general efficient synthetic procedure for the bis-(μ-oxo)bis-manganese(III) complexes has been devised so far.

In order to try to design more reliable manganese catalase models we decided to use tripodal ligands in which carboxylate donors could easily be introduced and to investigate the reactivities of the corresponding complexes. The ligands used in this study are depicted in Scheme 1. They involve successive replacements of pyridyl groups by carboxylate groups, going from tris-2-picolylamine (tpa) to bis-2-picolylglycylamine (Hbpg), to 2-picolyldiglycylamine (H_2pda), and finally to nitrilo-tris-acetic acid (H_3nta).

In this article we present the syntheses of the unknown bis-(μ-oxo)-bis-manganese(III,IV) complexes of the pda and nta ligands. We also describe a general one-electron reduction procedure to provide the bis-(μ-oxo)-bis-manganese-(III,III) compounds, which enabled us to obtain the tpa and Hbpg complexes. Finally we report on the influence of the carboxylate contents of the tripodal ligands on the properties and on the activities of the bis-(μ-oxo)-bis-manganese-(III,III) and -(III,IV) cores in the H_2O_2 disproportionation reaction. A comparison of the disproportionation activities of these complexes with their abilities to exchange their bridging oxygens with water emphasizes the dominating effect of the carboxylate group, which may act as an internal base, a feature likely to play an important role in the catalase-like reaction.

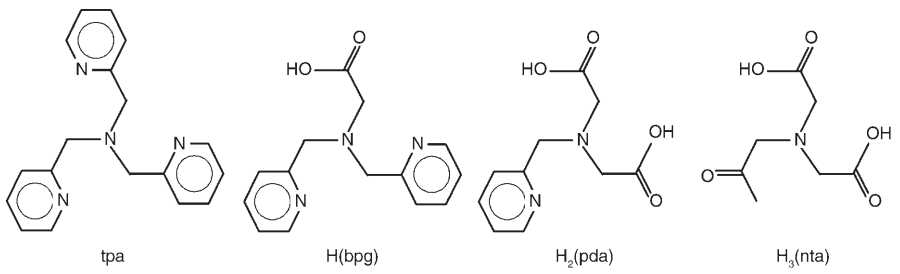

Scheme 1. Ligands used in this study.

Results

Syntheses

$Mn^{III}Mn^{IV}$ complexes: The $Mn^{III}Mn^{IV}$ complexes $[Mn_2(O)_2(tpa)_2](ClO_4)_3$ (**1**)[34] and $[Mn_2(O)_2(bpg)_2](ClO_4)$ (**2**)[35] had already been described. To assess the influence of a greater number of carboxylate ligands, as found in the catalase enzymes, we decided to extend this series of compounds to the corresponding complexes of the H_2pda and H_3nta ligands. However, all published synthetic procedures failed and led to manganese dioxide deposition, owing to the great instabilities of these compounds. The use of low temperatures (−20 °C for **3** and −60 °C for **4**) inhibited MnO_2 deposition and enabled us to obtain the two compounds $\{[Mn_2(pda)_2(O)_2]Na(H_2O)_6\}_n$ (**3**) and $[Mn_2(O)_2(nta)_2]Na_3$ (**4**) by treatment of the ligands with mixtures of manganese(II) nitrate and potassium permanganate. Compound **3** could be isolated in the solid state and crystallized,[36] but **4** proved to be too unstable to be obtainable as a solid and was therefore characterized only in solution at low temperature by EPR.

$Mn^{III}Mn^{III}$ complexes: The first bis(μ-oxo)bismanganese(III) complex was synthesized by Hodgson et al.[24] by use of the ligand 6-Mebispicen (*N*,*N*′-bis-(6-methylpicolyl)ethylenediamine) in the presence of manganese(II) perchlorate and oxygen, with a yield of 5%. The same group[26] prepared a series of such complexes by using ligands such as bisMepyren (*N*,*N*′-bis-(methyl-2-pyrazine)ethylenediamine) and tMepa (bis-(6-methyl-2-pyridylmethyl)(2-pyridylmethyl)-amine) and hydrogen peroxide as oxidizing agent with yields in the range from 30 to 76%. Using the same procedure, Mikata et al. very recently isolated such complexes in yields of around 30% with linear tetradentate quinoline ligands (*N*,*N*′-bis(2-quinolylmethyl)-*N*,*N*′-diethyl-ethylenediamine and its isopropyl analogue).[30] In 1994, Hodgson et al.[28] published the synthesis of the complex of the ligand bispicMe$_2$en (*N*,*N*′-bis-[(6-methylpicolyl)-(methyl)]ethylenediamine) by

reduction of the bis(μ-oxo)$Mn^{III}Mn^{IV}$ complex with sodium thiosulfate with a yield of 40%. Finally, Moro-oka et al. described the synthesis of the complex of the iprtpzb (isopropyltrispyrazolylborate) ligand by oxidation of the bis(μ-hydroxo) bis-manganese(II) complex either by oxygen or electrochemically with yields of around 50%.[27]

As a result of the observation that the bis(μ-oxo)-$Mn^{III}Mn^{IV}$ complexes are rather easily obtained, we decided to use them as precursors in a reductive procedure. We anticipated that the reaction should be easily monitored through EPR spectroscopy as the starting compounds possess the well known characteristic 16-line spectrum,[42] while the expected product would be EPR silent and the Mn^{II} products potentially obtained by "over-reduction" or disproportionation should be easily detectable through their characteristic six-line spectra.[43] As reducing agent we chose the benzil radical, because benzil is highly soluble in the reaction medium. By this method we succeeded in obtaining the bis(μ-oxo)-$Mn^{III}Mn^{III}$ complexes of the ligands tpa and Hbpg (**5** and **6**, respectively), from their bis(μ-oxo)-$Mn^{III}Mn^{IV}$ precursors.[34,35] With the ligand H_2pda the obtained complex disproportionated into $Mn^{III}Mn^{IV}$ and Mn^{II} derivatives over approximately a day at −20°C under argon. Owing to its neutrality, complex **6** could not be precipitated because of its strong solubility in all usual solvents, and its characterization by mass spectrometry was impossible. Moreover, over extended periods of time it started to disproportionate in solution. For all these reasons, we primarily studied the reactivity and the characterization of complex **5**. It is worth noting that this complex could not be obtained as described by Hodgson et al.[28] by reduction with sodium thiosulfate, which is a two-electron reducing agent and gave a mixture of different oxidation states. In contrast, the use of the benzil radical appeared quite general, and EPR monitoring showed a clean reduction of the $[Mn^{III}Mn^{IV}]$ without the appearance of other EPR active species. This indicates the formation of the desired $[Mn^{III}Mn^{III}]$ complexes in solution. Isolation of these complexes was only possible in the cases of **5** and **6**, owing to the intrinsic instability of the pda and nta derivatives with regard to disproportionation.

Solid state-characterizations

Crystal structure of 5: The structure of the dimanganese-(III,III) tpa complex **5** is illustrated in Figure 1. Crystal data are summarized in Table S1, and a selection of distances and angles is given in Table 1. Within the crystal, there is an alternation of planes of tetraphenylborate ions (BPh_4) and binuclear units in a BPh_4-cation-BPh_4-BPh_4-cation-BPh_4 arrangement. Each manganese is hexacoordinated, the coordination sphere being composed of four nitrogen atoms from the tpa ligand and two oxo bridges.

Table 1. Selected interatomic distances [Å] and angles [°] for **5**.

Mn–ligand distances			
Mn–O(1)	1.830(2)	Mn–O(2)	1.8324(18)
Mn–N(1)	2.188(3)	Mn–N(2)	2.342(2)
Mn–N(3)	2.322(2)	Mn–N(4)	2.092(2)
Σ[O–N(1)][a]	4.018	⟨Mn–L⟩	2.103
Σ[O–N(4)]	3.924	Mn–Mn	2.642(2)
Σ[N(2)–N(3)]	4.674	Mn-O-Mn	92.36(7)

[a] Σ: sum of Mn–ligand distances along a particular axis.

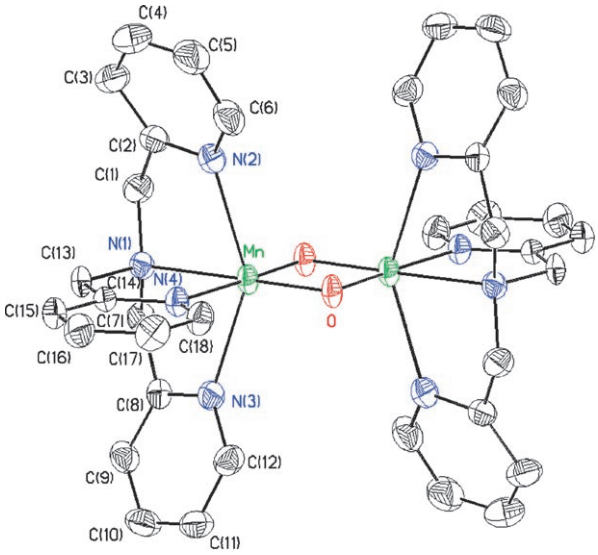

Figure 1. Structure of the dication $[Mn_2(tpa)_2(O)_2]^{2+}$ (**5**). Ellipsoids are drawn at 30% probability.

The structure obtained is very close to that of complex **1**.[34] The Mn_2O_2 diamond core is planar. Since the center of the Mn_2O_2 core is an inversion center, the manganese(III) ions are equivalent. The Mn–Mn distance in **5** is almost the same as in **1** (2.642 and 2.643 Å, respectively), in spite of the different redox states of the Mn pairs, thus showing a weak influence of the oxidation states in this case. This is the result of a lengthening of the $Mn–O_{oxo}$ distances (1.831 Å for **5** vs 1.807 for **1**) and a closing of the $Mn\text{-}O_{oxo}\text{-}Mn$ angle (92.36° for **5** vs 94.07 for **1**). Indeed, the two effects compensate each other, which ultimately leaves the Mn–Mn distance unaffected. A similar lengthening of the $Mn–O_{oxo}$ bonds with respect to **1** is observed for all other bond distances in **5** (corresponding average distance 2.103 Å for **5** vs 1.999 for **1**). The strongest effect is seen on the $Mn–N_{py}$ bond distances perpendicular to the Mn_2O_2 core, all four of them being elongated by the Jahn–Teller effect in **5** rather than only two in **1**.

Infrared spectroscopy

The complexes **1**–**3** and **5** were studied by infrared spectroscopy in order to investigate the influence of the ligands on the vibrations of the $Mn–O_{oxo}$ bonds. As expected, comparison of the spectra showed the progressive disappearance on going from **1** to **3** of the strong band at about 1100 cm^{-1} assigned to the perchlorate counter anion. Similarly, and more interestingly, the pyridine bands at about 3000–3150 cm^{-1} (aromatic CH), 1600 cm^{-1} (C=C pyridine), and 1560 cm^{-1}

(C=N pyridine) were replaced on going from **1** to **3** by those of the carboxylate groups: at 1624 cm^{-1} ($\nu_{C=O}$) and 1350 cm^{-1} (ν_{C-O}) for **2**, and at 1625 cm^{-1} ($\nu_{C=O}$), 1361 cm^{-1} (ν_{C-O}), and 1376 cm^{-1} (ν_{C-O}) for **3**. The differences between $\nu_{C=O}$ and ν_{C-O} carboxylate bands are 274 cm^{-1} for **2** and 264 cm^{-1} and 249 cm^{-1} for **3**. These values are characteristic of monodentate carboxylates.[44]

The vibrational properties of bis(μ-oxo)dimanganese cores have attracted much interest as a reference for interpreting those of various PSII S states.[45,46] From a number of IR and resonance Raman studies, as well as from normal coordinate analyses and recent DFT calculations, it follows that several vibrations in the 600–700 cm^{-1} range are associated with the Mn_2O_2 core. The IR spectra of complexes **1**–**3** and **5** were investigated in the solid state with the help of ^{18}O isotope substitution in order to locate the manganese oxo vibrations. Indeed, Cooper and Calvin described this type of infra-red spectroscopy experiment in the case of bis-(μ-oxo)$Mn^{III}Mn^{IV}$ bipyridine complexes.[47] They assigned a band at 676 cm^{-1} as the $Mn-O_{oxo}$ vibration. This band shifts by −12 cm^{-1} upon $^{16}O/^{18}O$ substitution. Similar observations were made by Czernuszewicz et al. by resonance Raman spectroscopy.[48] Indeed, a shift of about −30 cm^{-1} was observed for the $Mn-O_{oxo}$ vibration at 690 cm^{-1} upon $^{16}O/^{18}O$ exchange.

Theory predicts that for a bis(μ-oxo)$Mn^{III}Mn^{IV}$ complex of D_{2h} symmetry, two vibration modes (B_{2u} and B_{3u}), attributable to the oxo bridges, should be observable in infra-red spectroscopy. In the cases of **1**–**3**, only two bands proved sensitive to $^{16}O/^{18}O$ exchange (Figure S1). They are located at about 700 cm^{-1} (703, 697, and 694 cm^{-1}, respectively, for complexes **1**, **2**, and **3**) and 600 cm^{-1} (611, 605, and 610 cm^{-1}). Upon $^{16}O/^{18}O$ isotopic substitution, these bands shift by −25 cm^{-1}. The energy of the vibration mode at 700 cm^{-1} slightly decreases from **1** to **3**, reflecting a weakening of the associated bond, in agreement with the structural results (see below). This trend, however, is not observed for the other vibration mode at 600 cm^{-1}. The energies of these bands and their ^{18}O induced shifts compare favorably with those observed or calculated for various $Mn^{III}Mn^{IV}$ complexes.[49]

In the case of **5**, the assignment of the $Mn-O_{oxo}$ vibrations is less straightforward. Indeed, the main differences with **1** are located in the 500–800 cm^{-1} domain. Thus, the manganese−O_{oxo} vibrations, characteristic of $Mn^{III}Mn^{IV}$ complexes at 700 and 600 cm^{-1}, have disappeared. Isotopic exchange revealed that a band at 660 cm^{-1} narrows after labeling, whereas a band around 625 cm^{-1} becomes wider. It is thus likely that the $Mn-O_{oxo}$ vibration is located at 660 cm^{-1} and overlaps with a band at 657 cm^{-1}. Upon ^{18}O isotope substitution the $Mn-O_{oxo}$ vibration experiences a shift of −35 cm^{-1} and overlaps another band around 625 cm^{-1}, while the band at 657 cm^{-1} remains. To the best of our knowledge, there are no data in the literature for comparison. The lower energy of the vibration is consistent with the reduction of the oxidation state of the Mn_2O_2 core, and a 620 cm^{-1} energy has been calculated for $[Mn^{III}Mn^{III}(O)_2(NH_3)_8]^{2+}$.[49]

Magnetic susceptibility study

Numerous studies have shown that the magnetic properties of bis(μ-oxo)-$Mn^{III}Mn^{IV}$ complexes are dominated by the strong antiferromagnetic coupling ($-J \approx 130$–160 cm^{-1}) mediated by the oxo bridges, which couples the individual spins of the Mn^{III} and Mn^{IV} ions ($S=2$ and $S=3/2$, respectively) to an $S=1/2$ ground state.[28,31,35,50–53] We studied the magnetic properties of complexes **1**–**3** to assess the influence of the peripheral tetradentate ligand on the magnetic interaction. Owing to the strong coupling for all complexes and the small range of variation, it was necessary to study the three compounds in spite of earlier measurements on **1**–**2**.[35,50]

Figure S2 illustrates the temperature dependence of the magnetic susceptibilities for all compounds studied. In the cases of **1**–**3**, the product $\chi_M T$ is about 0.75 $K\,cm^3\,mol^{-1}$ at room temperature and decreases steadily with temperature until it reaches a plateau at $\chi_M T \approx 0.4$ $K\,cm^3\,mol^{-1}$, in agreement with an $S=1/2$ ground state (expected value for $\chi_M T \approx 0.375$ $K\,cm^3\,mol^{-1}$ for $g=2.0$). The experimental curves were simulated by use of the Van Vleck equation for two interacting spins $S=2$ and $S=3/2$ as described in the Experimental Section. Excellent simulations were obtained in all cases, and the best fit parameters are listed in Table 2. These fits reveal a trend in the exchange interaction, which becomes less antiferromagnetic in the order **1** ($-J=161\pm5$ cm^{-1}) < **2** ($-J=142\pm5$ cm^{-1}) < **3** ($-J=133\pm9$ cm^{-1}). As discussed below, this order parallels the strengths of the $Mn-O_{oxo}$ bonds, as revealed by the structural and infrared studies.

Table 2. Parameters deduced from simulation of the magnetic susceptibility data for **1**–**3** and **5**.

Complex	$-J$ [cm^{-1}]	g	TIP × 10^6 [$cm^3\,mol^{-1}$]	$10^4 \times I$[a]	R^2
1[b]	161 ± 5	2.00[c]	140 ± 10	17 ± 1	0.998
2[d]	142 ± 5	2.00[c]	120 ± 10	0	0.9993
3	133 ± 9	2.00[c]	10 ± 10	20 ± 1	0.998
5	106 ± 1	1.96	423 ± 10	10 ± 1	0.9997

[a] I corresponds to the molar content of contaminant spin $S=5/2$. [b] Literature value 159 cm^{-1}, ref. [50]. [c] Value fixed in the simulations. [d] Literature value 151 cm^{-1}, ref. [35].

The bis(μ-oxo)-$Mn^{III}Mn^{III}$ complexes experience a similar antiferromagnetic coupling, albeit less intense ($-J \approx 100$ cm^{-1}), as shown for complexes of the ligands 6-Mebispicen and bispicMe_2en.[24,28] The same behavior is observed for **5**. Between 300 and 60 K, the product $\chi_M T$ decreases from 1.00 $K\,cm^3\,mol^{-1}$ to 0.10 $K\,cm^3\,mol^{-1}$, reaching a plateau at lower temperatures, at a value of about 0.09 $K\,cm^3\,mol^{-1}$. The curve $\chi_M T = f(T)$ was simulated by using the Van Vleck equation adapted to two interacting spins $S=2$. An excellent fit was obtained with the parameters listed in Table 2. The antiferromagnetic exchange interaction deduced from the simulation ($-J=106\pm1$ cm^{-1}) is slightly higher than those

previously estimated for related compounds. As observed previously for the bis(μ-oxo)-$Mn^{III}Mn^{IV}$ complexes, the antiferromagnetic interactions parallel the strengths of the Mn–O_{oxo} bonds: [tpa] ($-J=106\ cm^{-1}$, Mn–$O_{oxo}=1.831$ Å) > [bispicMe2en][28] ($-J=101\ cm^{-1}$, Mn–$O_{oxo}=1.840$ Å) > [6]-Mebispicen,[24] ($-J=86\ cm^{-1}$, Mn–$O_{oxo}=1.849$ Å).

Solution studies

UV/Visible spectroscopy: The electronic absorption spectra of the bis(μ-oxo)-$Mn^{III}Mn^{IV}$ complexes are characterized by four bands located at about 15400, 18000, 22000, and 26000 cm^{-1}. In a very detailed analysis, Solomon et al. assigned the three lower energy transitions to an oxo→Mn^{IV} charge-transfer transition and two Mn^{IV} d–d transitions, respectively.[54] Similar assignments were proposed by Suzuki et al.[35] for **1** and by Hodgson et al.[24,28] for complexes of the bispicen and tpa series.

As shown in Figure 2 and Table 3, complexes **1–3** exhibit transitions in the expected domains. The shoulders around 380 nm (26315 cm^{-1}) do not move significantly on going from **1** to **3**, but rather decrease in intensity. This suggests that these bands can be assigned to $\pi \rightarrow \pi^*$ transitions within the pyridines of the ligands. On the other hand, the three other transitions exhibit a continuous trend to higher energy associated with the replacement of each pyridine by a carboxylate, in agreement with the substitution of an aromatic amine by an anionic oxygen ligand. This overall effect can be explained by considering the higher donating influence of carboxylates in relation to pyridines. As a consequence, the d orbitals of the Mn ions are more destabilized and the oxo to Mn charge transfer transition occurs at higher energy. Interestingly the spectra of **1** and **2** reveal an essentially constant displacement of all transitions, reflected by constant energy differences between them. Compound **3**, however, departs from this behavior, the energetic difference between bands II and III being increased. As pointed out by Solomon et al., this difference represents the splitting of the d_{xz} and d_{yz} orbitals due to out-of-plane interactions and directly reflects the extent of oxo-Mn^{IV} out-of-plane π bonding.[54] Comparison of the spectra of **1–3** fully supports this interpretation. Indeed, on going from **1** to **2** an in-plane pyridine is replaced by a carboxylate, and bands II and III are only shifted in energy by similar amounts. On the other hand, on going from **2** to **3** the replacement of an axial pyridine by a carboxylate causes a 20% increase in the splitting of bands II and III.

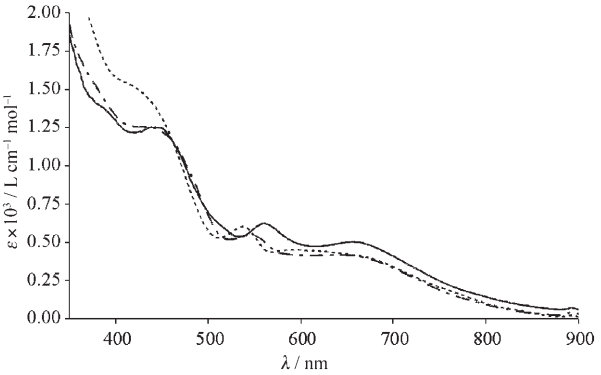

Figure 2. UV/visible spectra of compounds **1** (-----), **2** (–•–•), and **3** (——) in acetonitrile solution.

Table 3. Electronic absorption spectra of **1–3** in acetonitrile.

Complex	1	2	3
band I	660 (500)	640 (420)	590 (450)
λ [nm] (ε [L mol^{-1} cm^{-1}])	15152	15625	16949
E [cm^{-1}]			
band II	559 (621), 505 (650)	545 (550)	537 (600)
λ [nm] (ε [L mol^{-1} cm^{-1}])	17889; 19802	18349	18622
E [cm^{-1}]			
band III	439 (1250)	434 (1250)	413 (1550)
λ [nm] (ε [L mol^{-1} cm^{-1}])	22779	23041	24213
E [cm^{-1}]			
band IV	382 (1400)	380 (1480)	≈375
λ [nm] (ε [L mol^{-1} cm^{-1}])	26178	26316	≈26670
E [cm^{-1}]			

In contrast, **5** does not exhibit intense absorptions in the 350 to 800 nm range. The low extinction coefficients (between 100 and 360 L mol^{-1} cm^{-1}) of these bands lead to their assignment to d → d transitions. The oxo → Mn^{III} charge-transfer bands are probably located in the ultraviolet domain but cannot be observed owing to strong acetonitrile absorptions in this region.

EPR spectroscopy studies of $Mn^{III}Mn^{IV}$ complexes: Studies of complexes **1–4** by electron paramagnetic resonance were carried out on frozen solutions in acetonitrile in the presence of traces of DMF to improve the quality of the glass. The spectra of complexes **1** and **2** had already been described in the literature.[24,35] Nevertheless, we recorded them again in order to be able to make valuable comparisons of the various characteristics of these spectra. All spectra were recorded at low temperature (10 K) and are illustrated in Figure 3. The bis(μ-oxo)-$Mn^{III}Mn^{IV}$ complexes have a ground spin state $S=1/2$ owing to the strong antiferromagnetic coupling of the two ions of spins $S=2$ and $S=3/2$. Therefore, these compounds possess a signal centered at $g=2$. The hyperfine couplings with the ^{55}Mn nuclear spin result in a characteristic 16-line signal.[42] On varying the power of the microwave input, we noted a very fast signal saturation, even for low powers ($P > 6$ μW approximately). Experiments at various temperatures (4.5 to 40 K) did not indicate any change in the shape of the recorded spectrum, apart from a decrease in the intensity of the signal when the temperature was increased, consistently with the depopulation of the $S=1/2$ ground state. This shows that only the ground state is populated in the temperature range studied, as is to be expected owing to the large magnetic exchange coupling of the complexes (see above).

Table 4 reports the "best fit" parameters obtained from simulation of all spectra (Figure S3). The agreement factor

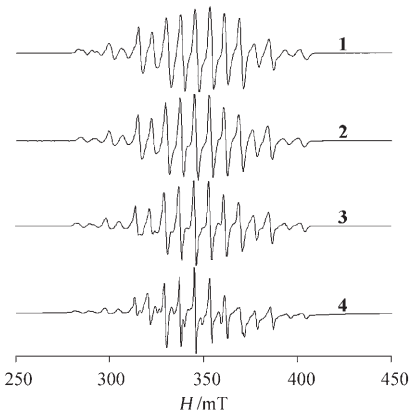

Figure 3. EPR spectra of compounds **1**–**4** in toluene/acetonitrile glass ($T=10$ K, $P=3.17$ μW, frequency modulation = 100 kHz, amplitude modulation = 9 G).

R (Table 4) is excellent for all complexes but complex **4**. The $|A_1|$ parameter is approximately double the $|A_2|$ parameter, which enables us to say that they represent the Mn^{III} and Mn^{IV} ions, respectively. The $|A_2|$ values are isotropic, whereas $|A_1|$ presents a rather important rhombicity. This anisotropy can be correlated with the distortion of Mn^{III} due to an important Jahn–Teller effect. In the same way, the g parameter is rather rhombic. For the series of complexes, the values of the parameters obtained are very close. We notice a slight increase in the g_{iso} and $|A_2|$ values on going from **1** to **4**. The parameters thus evaluated are of the same order of magnitude as those given in the literature for various bis(μ-oxo)$Mn^{III}Mn^{IV}$ complexes.[42] The parameter B, which corresponds to the half-width at middle height of the EPR lines, decreases by approximately 0.1–0.2 mT from **1** to **3** and, more importantly (ca. 0.35 mT), to **4**. This phenomenon is due to the reduction of the nitrogen hyperfine couplings when the pyridine ligands are replaced by carboxylate groups.

Table 4. Parameters deduced from the simulation of EPR spectra of **1**–**4**.

Complex		g	$\|A_1\|$ [10^{-4} cm^{-1}]	$\|A_2\|$ [10^{-4} cm^{-1}]	δB[a] [mT]	R[b]
1	x	2.000	159	68	1.1	0.004
	y	1.997	142	71		
	z	1.984	107	74		
	iso[c]	1.994	136	71		
2	x	2.001	154	70	1.0	0.01
	y	1.999	141	71		
	z	1.985	106	76		
	iso[c]	1.995	133	73		
3	x	2.004	157	72	0.85	0.01
	y	2.001	144	73		
	z	1.984	105	78		
	iso[c]	1.996	135	74		
4	x	2.007	160	73	0.5	0.22
	y	2.002	145	75		
	z	1.984	107	79		
	iso[c]	1.998	138	76		

[a] Spectral bandwidth (half-width at half-height). [b] Agreement factor: $R=\Sigma(I^{exp}-I^{calcd})^2/\Sigma(I^{exp})^2$. [c] $g_{iso}=(g_x+g_y+g_z)/3$.

Electrochemistry

The results obtained are presented in Table 5 and Figure 4. Complexes **1** and **2** each exhibit two reversible redox couples: one associated with the reduction of the complex in

Table 5. Electrochemical data for complexes **1**–**3**. Potentials are given in V vs $Ag/AgNO_3$ [10 mM].

Complex	Solvent	$Mn^{III/III}\rightleftarrows Mn^{III/IV}$	$Mn^{III/IV}\rightleftarrows Mn^{IV/IV}$
1	CH_3CN	$E_{1/2}=-0.05$	$E_{1/2}=+0.77$
		(+0.50[a])	(+1.32[a])
		$\Delta E_p=0.06$	$\Delta E_p=0.07$
2	CH_3CN	$E_{1/2}=-0.34$	$E_{1/2}=+0.43$
		(+0.21[a])	(+0.98[a])
		$\Delta E_p=0.08$	$\Delta E_p=0.10$
3	CH_3CN/H_2O (4:1)	$E_{pc}=-0.36$	$E_{1/2}=+0.37$
		(+0.19[a])	(+0.92[a])
		$\Delta E_p=0.10$	

[a] In parentheses value vs NHE, $\Delta E=+0.548$ V/Ag/Ag^+.

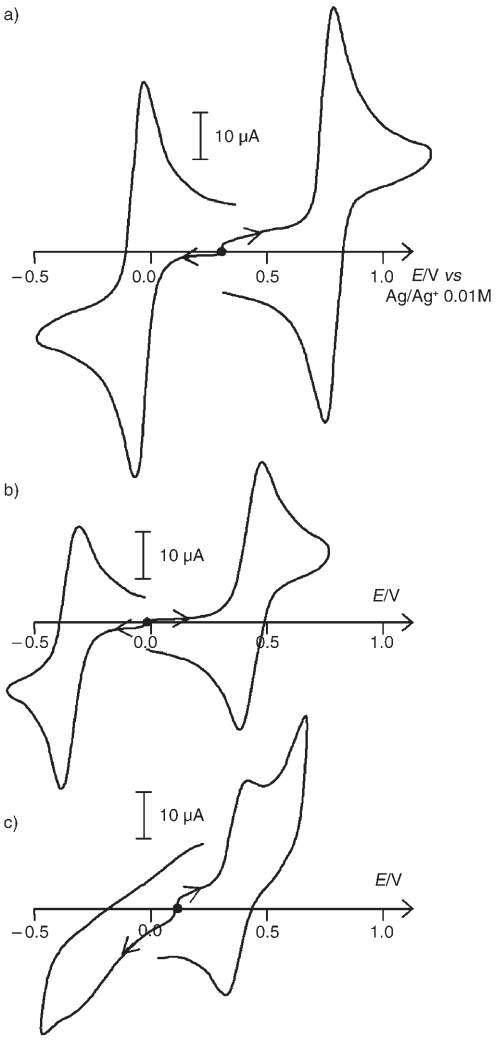

Figure 4. Cyclic voltammograms at a Pt electrode (diameter 5 mm) of: a) 0.9 mM solution of **1** in CH_3CN+TBAP (0.1 M), b) 0.6 mM solution of **2** in CH_3CN+TBAP (0.1 M), and c) 0.5 mM solution of **3** in CH_3CN/H_2O 4:1+TBAP (0.1 M). Sweep rate: 100 mV s^{-1}.

the bis(μ-oxo)-$Mn^{III}Mn^{III}$ species and another associated with its oxidation in the bis(μ-oxo)-$Mn^{IV}Mn^{IV}$ complex. In contrast, complex **3** presents only a reversible oxidation couple, the reduction being ill-defined. The potentials measured for complexes **1** and **2** are identical to those described in the literature.[24,35]

Examination of Table 5 shows that the replacement of one pyridine by a carboxylate group within the ligand lowers the oxidation potential of the $Mn^{III}Mn^{IV}/Mn^{IV}Mn^{IV}$ couple by 340 mV. A similar effect on the potential of the $Mn^{III}Mn^{III}/Mn^{III}Mn^{IV}$ couple (290 mV) is noted. The replacement of a second pyridine brings an additional, albeit smaller (60 mV), lowering of the oxidation potential. The better stabilization of the high oxidation state by the negatively charged carboxylate is responsible for these shifts in redox potentials. The reduced influence of the second carboxylate is probably caused by its location on the Jahn–Teller elongation axis of the Mn^{III} ion. The irreversibility of the reduction of complex **3** is probably due to the destabilization of its reduced $Mn^{III}Mn^{III}$ form by the anionic donors caused by the accumulation of two negative charges. It is consistent with the disproportionation observed during the benzil reduction of **3**.

Oxo exchange reactions: Because of the insolubility of **3** in acetonitrile, the exchange of oxo ligands was studied in acetonitrile/methanol (4:1) mixtures for **1**–**3** and **5** and in pure acetonitrile for **1**, **2**, and **5**. Figure 5 illustrates the time dependence of the disappearance of the starting compound upon treatment with 890 equiv of $H_2{}^{18}O$ monitored by electrospray ionization mass spectrometry. These results were obtained in acetonitrile/methanol 4:1; similar results were obtained in pure acetonitrile. For all complexes, ESI-MS revealed successive exchanges of the two oxo ligands (Figure S4) by the time-dependent disappearance of the isotopic pattern at $[M]$ of the unexchanged species by those at $[M+2]$ and $[M+4]$ of the singly and doubly exchanged species.

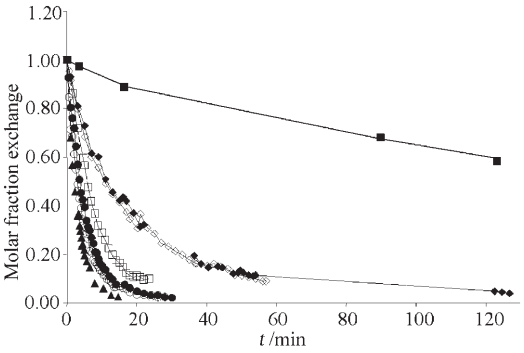

Figure 5. ESI-MS study of the exchange of oxo ligands in **1**–**3** with $H_2{}^{18}O$ in acetonitrile solution (**1**: ■, $+NEt_3$: □; **2**: ◆, $+NEt_3$: ◇; **3**: ▲, $+NEt_3$: △).

The data in Figure 5 could be simulated with a monoexponential law. Table 6 compares the oxo exchange kinetics of the compounds expressed as the times required for half-reaction of the starting compounds. These data show that the exchange in **1** is extremely slow ($t_{1/2} \approx 182$ min), but that replacement of a pyridine ligand in **1** by a carboxylate in **2** speeds up the exchange by more than an order of magnitude ($t_{1/2} \approx 14.4$ min for **2**). A second pyridine/carboxylate substitution further increases the rate about twofold ($t_{1/2} \approx 3.7$ min for **3**). As shown in Table 6, reduction of the $[Mn_2O_2]$ core from the mixed-valent state $[Mn^{III}Mn^{IV}]$ to the $[Mn^{III}Mn^{III}]$ state causes the rate to be increased by a factor of 84.

Table 6. Oxo exchange rates of complexes **1**–**3** and **5** in acetonitrile.

	Ligands[a]	$t_{1/2}$ [min]	Ligands[b]	$t_{1/2}$ [min]	$t_{1/2}$ [min] $+NEt_3$
$Mn^{III}Mn^{III}$			$(tpa)_2$, **5**	2.2	
$Mn^{III}Mn^{IV}$	$(mesterpy)_2(H_2O)_2$, **7**	4.6	$(dpa)_2$, **3**	3.7	3.1
	$(bpy)_2$, **8**	21.3	$(bpg)_2$, **2**	14.4	13.0
	$(phen)_2$, **9**	20	$(tpa)_2$, **1**	182.0	5.8
	$(bpea)_2(\mu\text{-}OAc)$, **10**	25.7			
$Mn^{IV}Mn^{IV}$	$(bpea)_2(\mu\text{-}OAc)$, **11**	231.7			

[a] Results from ref. [53]; bpea = bis-picolylethylamine, bpy = bipyridine, phen = 1,10-phenanthroline, mesterpy = mesitylterpyridine. [b] This work.

Since the oxo exchange reaction necessarily involves the deprotonation of a water molecule, the basic character of carboxylates could play a major role in the rate enhancement they bring about. To investigate this possibility the exchange reactions of compounds **1**–**3** in the presence of triethylamine were investigated. These experiments support this hypothesis. Indeed, the presence of triethylamine accelerates the oxo exchange of **1** by a factor of over 30 ($t_{1/2} \approx 5.8$ min) but has a limited effect on **2** and **3**. These observations strongly support the contention that a major contribution of the carboxylate ligands resides in their roles as internal bases.

Hydrogen peroxide disproportionation—kinetic studies on dimanganese(III,IV) complexes: As mentioned earlier, the oxidized forms of manganese catalases each contain a $[Mn^{III}{}_2O_2]$ core, which is believed to oxidize H_2O_2. Model $Mn^{III}(O)_2Mn^{IV}$ complexes with tpa, bpg, cyclam, and substituted bispicen ligands have shown activity in the catalase-like reaction.[55,56] Therefore the abilities of **1**–**3**, **5**, and **6** to disproportionate hydrogen peroxide were assessed in acetonitrile to evaluate the influence of the carboxylate ligands.

Figure 6 illustrates the time dependence of dioxygen evolution upon treatment of **1**–**3** with H_2O_2 at 0 °C. Lag phases are observed for the less reactive compounds **1** and **2**. As can be seen from Figure 6, **3** and **2** disproportionate 460 equivalents of H_2O_2 in about 40 and 110 min, respectively, but **1** would require about 7 h to achieve it. This translates into very different maximum dioxygen evolution rates, from

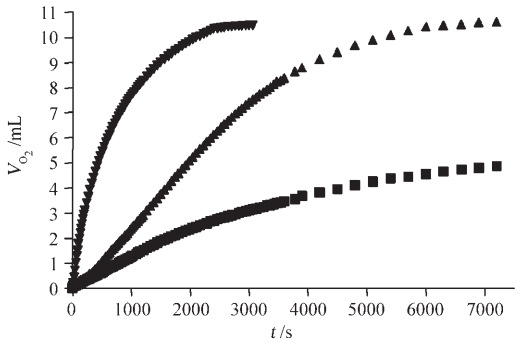

Figure 6. Hydrogen peroxide disproportionation by compounds **1** (▼), **2** (▲), and **3** (■) in acetonitrile. Conditions: [complex]: 1 mM, [H_2O_2]: 460 mM, $T = 0$ °C.

$V_{max} = 0.04 \pm 0.01$ mL min^{-1} for **1**, to 0.18 ± 0.05 mL min^{-1} for **2**, and to 1.0 ± 0.1 mL min^{-1} for **3**. The partial orders of the reaction were investigated for **1**–**3** and were shown to be close to 1 for the complex and H_2O_2.

The influence of acid/base addition was then investigated at 20 °C with 230 equiv H_2O_2 (under these conditions $V_{max} = 0.09 \pm 0.01$ mL min for **1** and 0.4 ± 0.05 mL min for **2**) and is depicted for **1** in Figure 7. Addition of 1 equivalent $HClO_4$ has a strong inhibitory effect on the reaction of **1** ($V_{max} = 0.02 \pm 0.005$ mL min^{-1}). In contrast, addition of triethylamine causes a significant enhancement of the rate, which reaches $V_{max} = 1.0 \pm 0.1$ mL min^{-1} at one equivalent NEt_3 and $V_{max} = 4.0 \pm 0.4$ mL min^{-1} at two equivalents NEt_3. A qualitatively similar effect is observed for **2**, but the enhancement factor brought about by two equivalents of NEt_3 is reduced to 7 ($V_{max} = 2.9 \pm 0.3$ mL min^{-1}), in comparison with 44 for **1**. It is noteworthy that the maximum rate for **2** under these conditions is close to that determined for **3** in the absence of base ($V_{max} = 2.5$ mL min^{-1}).

Dimanganese(III,III) complexes: Similar studies were performed with **5** and **6**, the dimanganese(III) complexes of tpa and Hbpg ligands, respectively. Both compounds exhibit behavior qualitatively similar to that of their dimanganese(III,IV) counterparts but with a dramatically enhanced activity (Figure S5). Indeed, at 0 °C and 230 equiv H_2O_2, under the conditions of Figure 6, the maximum disproportionation rate observed for **5** amounted to $V_{max} = 0.60 \pm 0.05$ mL min^{-1}, 30 times that of **1** under the same conditions ($V_{max} = 0.02 \pm 0.005$ mL min^{-1}). Only a 15-fold enhancement was observed for **6** vs **2**: $V_{max} = 1.40 \pm 0.05$ mL min^{-1} ($V_{max} = 0.09 \pm 0.005$ mL min^{-1} for **2** under the same conditions). As in the dimanganese(III,IV) complexes, replacement of a pyridine by a carboxylate accelerates the disproportionation reaction, but this effect is reduced. Partial orders with respect to **5** and H_2O_2 were estimated as 1 from the concentration dependences.

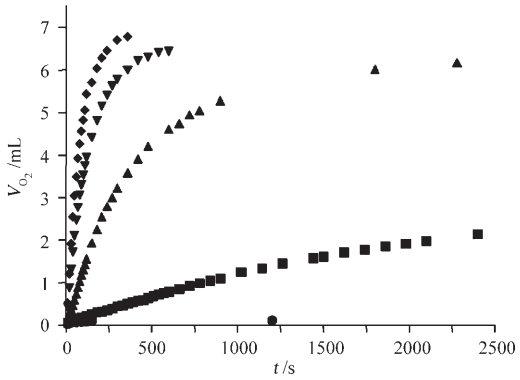

Figure 7. Influence of the addition of acid and base on the disproportionation rate of H_2O_2 by complex **1** in acetonitrile. Conditions: [complex]: 1 mM, [H_2O_2]: 230 mM, $T = 20$ °C, in the presence of 0 equiv (■), 1 equiv (▲), 2 equiv (▼), and 4 equiv (◆) NEt_3 and 1 equiv of perchloric acid (●).

In the case of **5**, addition of one equivalent $HClO_4$ slows down the disproportionation rate fivefold ($V_{max} = 0.12 \pm 0.01$ mL min^{-1}). As observed for **1**, addition of one and two equivalents of NEt_3 accelerates the reaction rate of **5** to $V_{max} = 1.6 \pm 0.1$ mL min^{-1} and 2.2 ± 0.1 mL min^{-1}, respectively. On the contrary, addition of one equivalent of NEt_3 has no effect on the reaction rate of **6** ($V_{max} = 1.44 \pm 0.05$ mL min^{-1}, Figure S6).

To summarize these observations, the intrinsic activities of the complexes decrease in the order **6** > **5** > **3** > **2** > **1**, being favored by a lower oxidation state of the Mn pair ($Mn^{III}Mn^{III} > Mn^{III}Mn^{IV}$) and by carboxylate ligands. These activities are drastically enhanced by the addition of base. Interestingly, however, this base enhancement of the catalase-like activity is more important for the less active compounds.

Spectroscopic monitoring

Dimanganese(III,IV) complexes: The disproportionation reactions were studied by a combination of mass spectrometry and UV/Visible and EPR spectroscopy in the hope of detecting key intermediates, as had also been done earlier.[22,23] In the cases of the dimanganese(III,IV) complexes **1**–**3**, progressive disappearance of the starting compound was noted through a continuous decrease in the three characteristic bands in the visible region and of the 16-line EPR spectrum. In the final stage of the reaction this spectrum is superimposed on a broad, featureless component extending from 250 to 450 mT. Similar characteristics have been associated with dimanganese(II,III) species[22,57,58] At the end of the reaction the 16-line spectrum had vanished, and a poorly resolved six-line EPR spectrum was superimposed on the broad component, indicating the formation of Mn^{II} species.

The formation of Mn^{II} species was also evidenced by ESI-MS monitoring, as depicted in Figure 8. Complex **2** gives rise to a peak at m/z 654 corresponding to the monocation $[Mn_2^{III,IV}(\mu\text{-}O)_2(bpg)_2]^+$. After addition of H_2O_2, three peaks appeared at m/z 311, 744, and 892 and were assigned the formulas $[Mn^{II}(bpg)]^+$, $[Mn_2^{II}(bpg)_2(pic)]^+$, and $[Mn_2(bpg)_2(bpgO)]^+$, respectively, where Hpic and HbpgO are 2-picolinic acid and *N*-picolyl-*N*-picolinamidoglycine, respectively

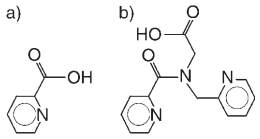

Scheme 2. Structures of 2-picolinic acid (a) and *N*-picolyl-*N*-picolinamidoglycine (b).

(Scheme 2). The last two formulas match the *m*/*z* values for the peaks but they are only tentative. Nevertheless, this indicates that during the disproportionation reaction the ligand may be oxygenated on one benzyl-like position, which is notoriously sensitive. The resulting amide group in HbpgO could be hydrolyzed to 2-picolinic acid.

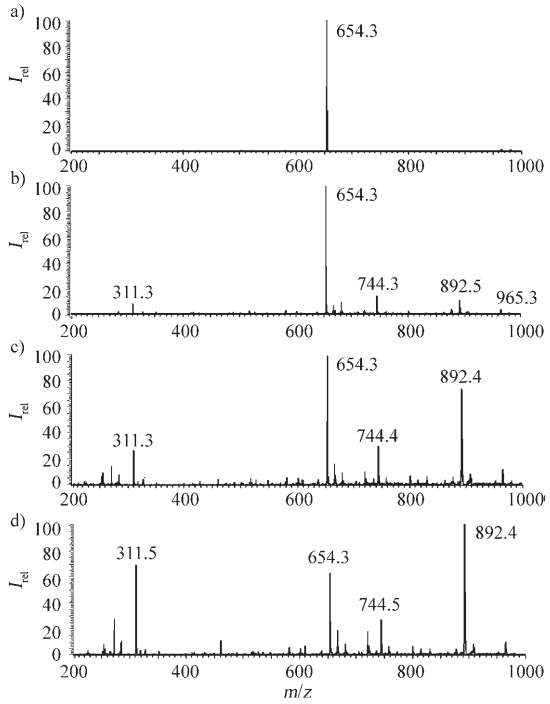

Figure 8. ESI-MS monitoring of the disproportionation reaction of complex **2** in acetonitrile. Conditions: [complex]: 1 mM, [H_2O_2]: 460 mM, T = 20 °C. a) t = 0 min, b) t = 1.2 min, c) t = 10 min, d) t = 20 min.

To provide further insight into the mechanism of the disproportionation reaction, **2** was treated with ^{18}O-labeled hydrogen peroxide ($H_2{}^{18}O_2$ at 3% in $H_2{}^{16}O$). Figure 9 illustrates the results of ESI-MS monitoring of the reaction. It shows that 1 min after $H_2{}^{18}O_2$ addition the peak of singly ^{18}O-labeled **2** equals that of unlabeled **2**, but that after 10 min this peak has lost intensity, probably after exchange with the unlabeled water present in the medium. This experiment shows that **2** incorporates oxo ligands from H_2O_2, which suggests that it belongs to the catalytic cycle and that it is most probably the oxidized form of the catalytic system.

Dimanganese(III,III) complexes: More limited spectroscopic monitoring was performed with **5**, owing to the fact that it is EPR silent and possesses a weak and almost featureless UV/Visible spectrum. Interestingly, however, when the reaction between **5** and H_2O_2 was followed by EPR spectroscopy

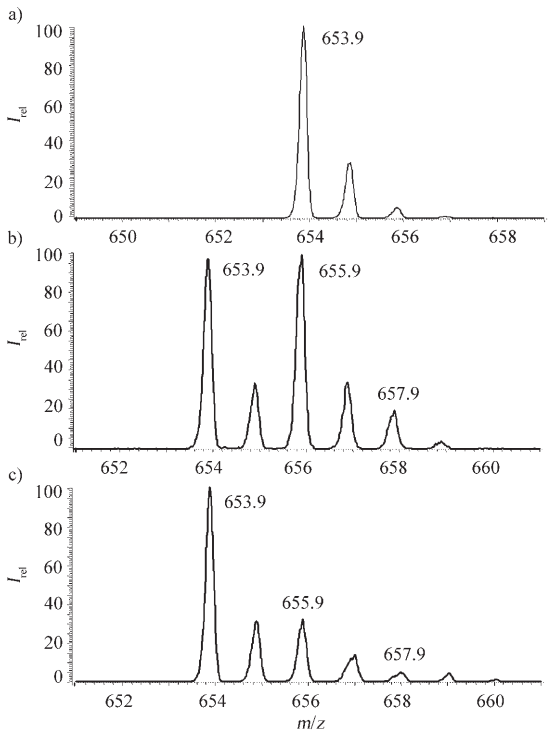

Figure 9. ESI-MS monitoring of the disproportionation reaction of complex **2** in acetonitrile. Conditions: [complex]: 1 mM, [H_2O_2]: 460 mM, T = 20 °C. a) Spectrum of **2**, b) after 1 min reaction time with $H_2{}^{18}O_2$ (3% in H_2O), c) same after t = 10 min.

the 16-line spectrum characteristic of **1** developed over the first 10 min before subsiding to a six-line spectrum, which was fully formed after 20 min. Quantitation of the 16-line spectrum shows that at its maximum it represents about 15% of the initial concentration of **5**. ESI-MS monitoring confirmed that the disproportionation reaction produced **1**, which appeared as a monocation $[Mn_2{}^{III,IV}(\mu\text{-}O)_2(tpa)_2(ClO_4)_2]^+$ at *m*/*z* 919. Two additional peaks appeared at *m*/*z* 362 and 467 and can be assigned to the Mn^{II} species $[Mn(tpa)(OH)]^+$ and $[Mn(tpa)(pic)]^+$, respectively. As observed for **2** when the reaction was run with $H_2{}^{18}O_2$, **5** incorporates oxo ligands from the peroxide, as is shown by an increased contribution of the peaks at 823 and 825 in relation to that of unlabeled **5** at 821. As above, this experiment suggests that **5** is the active oxidized species. The possibility that **1** is the actual catalyst is ruled out by its slower disproportionation rate (see above).

Discussion

Electronic properties: The replacement of pyridine ligands by carboxylates has a significant but limited effect on the electronic structures of the dimanganese(III,IV) bis-(μ-oxo) complexes **1**–**3**. Indeed, the continuous compensation of the metal charge by the terminal ligand induces a small expansion of the $[Mn_2O_2]$ core, as evidenced by the lengthening of the Mn–Mn bond distances (**1**: 2.643 Å < **2**: 2.656 Å < **3**:

2.667 Å). This expansion of the $[Mn_2O_2]$ core is due to a small elongation of the Mn–O_{oxo} bond distances (**1**: 1.807 Å < **2**: 1.810 Å < **3**: 1.818 Å), with the Mn-O-Mn angles remaining essentially constant at 94.4(5)°. As a consequence, the stretching frequency of the Mn–O_{oxo} bond diminishes slightly (703, 697 and 694 cm^{-1}, respectively, for complexes **1**, **2**, and **3**). Consistently, the intensity of the antiferromagnetic exchange coupling also diminishes (**1**: $-J = 161\ cm^{-1}$ < **2**: $-J = 142\ cm^{-1}$ < **3**: $-J = 133\ cm^{-1}$). This latter effect reflects the reduction of the overlap between the oxo and the manganese magnetic orbitals due to the Mn–O_{oxo} bond lengthening.[40]

Carboxylate replacement of a pyridine ligand has a dramatic influence on the redox potentials of the Mn_2O_2 core, which exhibit a significant lowering consistent with the increase in the negative charge of the complexes. Nevertheless the strength of this effect varies. Indeed, substitution of an in-plane pyridine in **1** by a carboxylate in **2** lowers both the oxidation and the reduction potentials of the $Mn^{III}Mn^{IV}$ unit by about 300 mV. In contrast, substitution of an axial pyridine in **2** by a carboxylate in **3** reduces the oxidation potential by only 60 mV. A possible explanation for this difference may lie in the different coordination sites of the two carboxylates: while the first one (in **2**) binds in the plane of the $[Mn_2O_2]$ core and is *trans* to one oxo bridge, the second (in **3**) occupies a *cis* position, which is axial and therefore lies on the Jahn–Teller elongation axis. As a consequence of this distortion, the axial carboxylate interacts with the Mn ion less strongly (Mn–O_{carb} 2.09 Å) than the in-plane one (Mn–O_{carb} 1.96 Å), which may be the basis of their strikingly different redox influences.

Oxo exchange: Tagore et al. have recently reported on the oxo exchange in di(μ-oxo)dimanganese(III,IV) and (IV,IV) complexes.[59,60] They showed that i) the exchange is strongly influenced by the ligand *trans* to the oxo, ii) it is favored by the presence of a labile coordination site, iii) it requires ligand dissociation when the manganese coordination is saturated by chelating ligands, and iv) it is favored by the binding of anions that lower the positive charge on the manganese ions. In addition, the exchange is more than ten times faster on Mn^{III} than on Mn^{IV}. Their results are summarized and compared to those from this work in Table 6, which presents the exchange efficiency as the time required for half exchange of the oxo ligands.

The tripodal parent compound **1** exchanges its oxo ligands one order of magnitude more slowly than the complexes of bis(diamino) ligands **8** and **9**. This shows that the tripodal amine is more difficult to dissociate than the bidentate diimines. The exchange reaction is drastically speeded up (ca. 13 times) by the introduction of an in-plane carboxylate in **2** occupying a coordination site *trans* to one oxo ligand. Introduction of a second carboxylate in **3** brings a further about fourfold acceleration of the oxo exchange. As a result of these two pyridine/carboxylate substitutions the oxo exchange rate surpasses that of compound **7**, which possesses an easily exchangeable coordination site. This emphasizes that carboxylates contribute to drastically increasing the oxo exchange rate in these dimanganese(III,IV) complexes.

This effect is quantitatively more important than could have been predicted from the modest Mn–O_{oxo} bond lengthening observed in the **1**/**2**/**3** series. Indeed, the associated weakening of the Mn–O_{oxo} bond is far too small to be responsible for the strong reactivity changes. This suggests that the carboxylate may play a more active role than strict charge compensation. Indeed it may be envisaged that owing to their intrinsic lability the carboxylate ligands dissociate,[59] thus opening a coordination site for an incoming water molecule. Such an effect would be more important for an axial carboxylate bound on the Jahn–Teller elongation axis than for an in-plane carboxylate. This is not consistent with the observation of a major effect of the in-plane carboxylate in **2** and the importance of in-plane ligands stressed by Tagore et al.[59,60] We are thus led to envisage that the in-plane carboxylate ligand may act in a more specific way. At this point it is worth noting that addition of triethylamine induces a rate increase in the exchange reaction similar to that produced by the replacement of a pyridine by an in-plane carboxylate. This suggests that the carboxylate ligands may play the role of internal bases, assisting the deprotonation of the substrate. In the oxo exchange reaction, the in-plane carboxylate may interact with the incoming water, thereby assisting its deprotonation to the strongly bound hydroxide. Proton transfer to the oxo ligand and re-binding of the carboxylate would produce a dihydroxo species with a single oxo bridge. Elimination of water would then reconstitute the second oxo bridge either isotopically normal or exchanged.

When comparing compounds **10** and **11**, Tagore et al. concluded that oxo exchange on Mn^{IV} is about 10 times slower than on Mn^{III}. This effect is drastically enhanced when dimanganese(III,III) systems are considered. Indeed, the comparison of **1** and **5** reveals an 83-fold enhancement of the rate on going from $Mn^{III}Mn^{IV}$ to $Mn^{III}Mn^{III}$ tpa complexes. These results thus fully agree with the observations and conclusions of Tagore et al.,[59,60] but while the same overall trends are observed the various effects appear to be strongly enhanced by the carboxylates, pointing to a specific role of these ligands.

Hydrogen peroxide disproportionation: Interestingly, on going from **1** to **2** to **3**, each carboxylate/pyridine substitution increases the disproportionation rate fivefold. Completely different shifts in the oxidation potentials are observed, since they are markedly reduced on going from **1** to **2** but far less on going from **2** to **3**. This different behavior indicates that the redox potential lowering cannot be the origin of the disproportionation rate increase. It is noteworthy that carboxylate/pyridine substitution induces a similar rate enhancement in the oxo bridge exchange, which is a non-redox process (see below). As detailed above, a rate enhancement similar to that of carboxylate can be brought about by the addition of triethylamine, but this effect is reduced as the number of carboxylate ligands increases. This

suggests that the carboxylates may play the role of internal bases in assisting the deprotonation of H_2O_2. In this respect the carboxylate arms of these ligands may mimic Glu65 and Glu148 when bound to manganese ions, or Glu178 when unbound. Glu65 and Glu148 are indeed Mn ligands in *Lactobacillus plantarum* catalase, while Glu178 resides in the close vicinity of the dimanganese unit.[7] All these glutamate residues are strongly H-bonded to water/hydroxide bridges and terminal water ligand in the reduced state of the enzyme and have been postulated to assist the enzyme in H_2O_2 deprotonation.

Conclusion

We have described here a new and general synthetic route to dimanganese(III,III) complexes through benzil reduction of the corresponding readily available dimanganese(III,IV) precursors. In this respect we have systematically introduced carboxylates in place of pyridines into tripodal ligands in order to assess the influence of this substitution. Indeed, aspartate and glutamate are always found as manganese ligands in proteins and their true influence was not precisely assessed through biomimetic chemistry. This influence proved to be drastic in oxo exchange and hydrogen peroxide disproportionation reactions. Indeed, in both cases, carboxylate introduction leads to a strong increase in the reaction rate, and this effect may probably be assigned to the ability of carboxylate ligands to act as internal bases. This effect is likely to be important in the catalase reaction, in which hydrogen peroxide must be deprotonated and the protons transferred to oxo ligands to eliminate water molecules. Indeed, it has recently been shown that the assistance of proton transfer, in particular in a concerted manner, is crucial to many electron transfers and, moreover, that carboxylate residues can act as proton acceptor groups in theses processes.[61]

Experimental Section

Materials: All solvents and reagents were of the highest quality available and were used as received unless noted otherwise. THF and acetonitrile were heated at reflux over sodium/benzophenone and phosphorus pentoxide, respectively, and were distilled immediately before use. $H_2{}^{18}O$ (95% ^{18}O) and $H_2{}^{18}O_2$ (90% ^{18}O, 2.2% in H_2O) were obtained from Eurisotop and Leman, respectively. The concentrations of H_2O_2 stock solutions were determined monthly through permanganate titration. H_3nta was purchased from Sigma, and tpa,[32] Hbpg,[33] and H_2pda[33] were prepared by literature procedures. Compounds **1** $[Mn_2(O)_2(tpa)_2](ClO_4)_3$ and **2** $[Mn_2(O)_2(bpg)_2](ClO_4)$ were prepared by literature procedures.[34,35]

Synthesis

$\{[Mn_2(pda)_2(O)_2]Na(H_2O)_6\}_n$ (3):[36] In an Erlenmeyer flask, H_2pda (0.112 g, 0.5 mmol) was neutralized with a saturated solution of sodium hydrogencarbonate. Acetone (15 mL) was added, and the solution was cooled down to −20 °C. A chilled solution of manganese(II) nitrate (60 mg, 0.35 mmol) in acetone was then added, followed by a solution of 23 mg (0.15 mmol) of potassium permanganate in the minimum possible amount of water. The resulting green-black solution was evaporated under vacuum at low temperature, and the resulting product was washed with acetonitrile and crystallized at −20 °C from a 50:50 mixture of acetone and water to produce green black needles (100 mg, yield: 65%). Mass spectrometry (ESI-MS$^-$): m/z: 586 $[M-Na]^-$.

$[Mn_2(O)_2(nta)_2]Na_3$ (4): In an Erlenmeyer flask, H_3nta (0.095 g, 0.5 mmol) was neutralized with a saturated solution of sodium hydrogencarbonate. Acetone (15 mL) was added, and the solution was cooled down to −60 °C. A chilled solution of manganese(II) nitrate (60 mg, 0.35 mmol) in acetone was then added, followed by a solution of potassium permanganate (23 mg, 0.15 mmol) in the minimum possible amount of water. The resulting green-black solution was analyzed directly by EPR spectroscopy.

$[Mn_2(O)_2(tpa)_2](BPh_4)_2$ (5): This synthesis was performed in a glove box under argon. In a flask, **1** (100 mg) were dissolved in anhydrous acetonitrile (150 mL). Simultaneously, a solution of the benzil radical was prepared by adding a piece of freshly cut sodium to a solution of benzil (1 g) in anhydrous THF (10 mL). The benzil radical solution turned orange immediately. The two solutions were cooled down to −20 °C, and aliquots of the benzil radical solution were added to that of **1**. The reaction was monitored by EPR by observation of the disappearance of the 16-line signal of **1**. When this signal had completely vanished, an acetonitrile solution of sodium tetraphenylborate (500 mg) was added, causing the appearance of small orange brown crystals (100 mg, 75%). Mass spectrometry (ESI-MS$^+$): m/z: 1040 $[M-BPh_4]^+$.

$[Mn_2(O)_2(bpg)_2]$ (6): This synthesis was performed from **2** (50 mg) as described for **5**. When the EPR signal of **2** had totally vanished, the solvent was stripped off within the glove box, and the recovered solid was washed with THF. It was then dissolved in acetone and filtered to remove insoluble impurities. Evaporation of the solvent gave **6** (30 mg, yield: 65%).

Caution! Perchlorate salts of metal complexes with organic ligands are potentially explosive

X-ray crystallography: The diffraction data for compound **5** were taken at room temperature with a Bruker SMART CCD area detector three-circle diffractometer ($Mo_{K\alpha}$ radiation, graphite monochromator, λ = 0.71073 Å).

The values of the cell parameters were refined by use of the SAINT program,[37] and the data were processed with the SADABS Bruker program.[37] Complete information on crystal data and data collection parameters is given in the Supporting Information. The structure was solved by direct methods by use of the SHELXTL 5.03 package,[38] and all atoms were found by difference Fourier syntheses. All non-hydrogen atoms were anisotropically refined on F^2. Hydrogen atoms were included in calculated positions.

CCDC 656465 contains the supplementary crystallographic data for this paper. These data can be obtained free of charge from The Cambridge Crystallographic Data Centre via www.ccdc.cam.ac.uk/data_request/cif

Spectroscopic measurements: Electronic absorption spectra were recorded on a Hewlett–Packard HP 89090 A or 8452 A diode array spectrophotometer. Infrared spectra were recorded with a Perkin–Elmer 1600 FTIR spectrometer, as dispersions (1–1.5 wt%) of the compounds in KBr.

EPR spectra at X band were recorded with an EMX Bruker spectrometer fitted with an Oxford Instruments ESR900 cryostat. All spectra presented were recorded under unsaturated conditions with the following set of parameters: T = 10 K, P = 3.17 μW, frequency modulation = 100 kHz, amplitude modulation = 9 G. Simulation of the EPR spectra was performed as already described.[39] ^{1}H and ^{13}C NMR spectra were recorded on a Bruker AC 200 spectrometer with a characteristic absorption of the solvent as internal reference. Electrospray ionization mass spectra were obtained with a LCQ Finnigan Thermoquest ESI source spectrometer with an ion trap and an octupolar analyzer.

Magnetic measurements: The magnetic susceptibilities of compounds **1**, **2**, **3**, and **5** were measured over the temperature range 5–300 K at 0.5 and 5 T. The samples (ca. 10 mg) were contained in a kel F bucket that had been independently calibrated. The data were corrected from diamagnetism by use of Pascal's constants.[40] The data were simulated by use of the Van Vleck equations derived from the Heisenberg exchange Hamiltonian

($H=-2J\hat{S}_1\hat{S}_2+\beta_e\hat{H}\breve{g}\hat{S}$).[40] Equation (1) was used for compounds **1**–**3** and Equation (2) for **5**:

$$\chi_m T = 0.094\, g^2 \frac{1+10\exp(3x)+35\exp(8x)+84\exp(15x)}{1+2\exp(3x)+3\exp(8x)+4\exp(15x)} + tT \qquad (1)$$

$$\chi_m T = 0.75\, g^2 \frac{\exp(2x)+5\exp(6x)+14\exp(12x)+30\exp(20x)}{1+3\exp(2x)+5\exp(6x)+7\exp(12x)+9\exp(20x)} + tT \qquad (2)$$

with $x=J/(k_BT)$ and t standing for the temperature-independent paramagnetism. The R indexes were 0.99886, 0.99932, 0.99896, and 0.999791 for **1**–**3** and **5**, respectively.

Electrochemistry: All electrochemical experiments were run under argon in a dry glovebox at room temperature, with a standard three-electrode electrochemical cell.[41] The electrolyte was a solution of tetra-*n*-butylammonium perchlorate (TBAP, 0.1 M, Fluka (puriss)) in acetonitrile (Rathburn, HPLC grade S). Potentials were referred to an $Ag/AgNO_3$ (10 mM) reference electrode in CH_3CN (+0.1 M TBAP). Potentials referred to this system can be converted to the ferrocene/ferrocenium couple by subtracting 87 mV, or to SCE or NHE by adding 298 or 548 mV, respectively. The working electrode was a platinum disc (diameter 0.25 cm) polished with 2 μm diamond paste for cyclic voltammetry (E_{pa}, anodic peak potential; E_{pc}, cathodic peak potential; $E_{1/2}=(E_{pa}+E_{pc})/2$; $\Delta E_p=E_{pa}-E_{pc}$). Electrochemical measurements were carried out with an EG G PAR model 173 potentiostat fitted with a model 179 digital coulometer and a model 175 programmer with output recorded on a Sefram TGM 164 *X*–*Y* recorder.

Kinetic experiments: In a typical oxo exchange reaction, a solution of complex (1 mM, 1 mL) was treated with $H_2{}^{18}O$ (16 μL) and the reaction was monitored by ESI-MS. For every compound at every time, the peaks at M (unexchanged), $M+2$ (singly exchanged), and $M+4$ (doubly exchanged) were integrated. The integrals of the singly exchanged species at $M+2$ were corrected for the contributions of the unexchanged species. Similarly, the integrals of the doubly exchanged species at $M+4$ were corrected for the contributions of the unexchanged and the singly exchanged species. The kinetic data were fitted to a monoexponential law $[Mn_2O_2]=C_0\exp(-k\times t)$ with agreement factors higher than 0.99.

The rate constants of the catalase-like reactions were determined by volumetric measurements of the evolved dioxygen. The whole apparatus, built from borosilicate glass, was kept at a constant temperature (± 0.2 °C) by use of a thermostatted ethanol circulation bath (Haake FQ-4). In a standard procedure, catalyst solution (2 mL) was placed in the kinetic apparatus. The solution was stirred for 30 min to reach a stable temperature. The chosen volume of hydrogen peroxide stock solution was added, and the volume of evolved dioxygen was then measured as a function of time. To compare the kinetics at different temperatures, the volume of the gas was converted to a reference temperature (273 K) by use of the ideal gas law. The volume was also corrected for the vapor pressure of the solvent at the working temperature by use of the expression $V_{corr}=V_{mes}(P_{atm}-P_{vap})/P_{atm}$, where V_{corr} is the corrected volume, V_{mes} the measured volume, P_{atm} the atmospheric pressure, and P_{vap} the vapor pressure of the solvent at the working temperature. In most cases, the initial rates were obtained by measuring the slopes of the tangents of the curve $v(O_2)$ vs time at 0 s. When a lag phase was present (i.e. experiments with **1a** at low H_2O_2 concentrations), the steepest slope after the initiation phase was used.

Acknowledgement

Dr. G. Blondin is gratefully acknowledged for a careful reading of the manuscript. This research was supported by the COST D21 program.

[1] B. Halliwell, J. M. C. Gutteridge, *Meth. Enzymol.* **1990**, 1–85.
[2] E. R. Stadtman, P. B. Berlett, P. B. Chock, *Proc. Natl. Acad. Sci. USA* **1990**, *87*, 384–388.
[3] Y. Kono, I. Fridovich, *J. Biol. Chem.* **1983**, *258*, 6015–6019.
[4] G. S. Allgood, J. J. Perry, *J. Bacteriol.* **1986**, *168*, 563–567.
[5] V. V. Barynin, A. I. Grebenko, *Dokl. Akad. Nauk SSSR* **1986**, *286*, 461–464.
[6] S. V. Antonyuk, V. R. Melik-Adamyan, A. N. Popov, V. S. Lamzin, P. D. Hempstead, P. M. Harrison, P. J. Artymyuk, V. V. Barynin, *Crystallogr. Rep.* **2000**, *45*, 105–116.
[7] V. V. Barynin, M. M. Whittaker, S. V. Antonyuk, V. S. Lamzin, P. M. Harrison, P. J. Artymiuk, J. Whittaker, *Structure* **2001**, *9*, 725–738.
[8] L. Le Pape, E. Perret, I. Michaud-Soret, J. M. Latour, *J. Biol. Inorg. Chem.* **2002**, *7*, 445–450.
[9] I. Michaud-Soret, L. Jacquamet, N. Debaecker-Petit, V. V. Barynin, J. M. Latour, *Inorg. Chem.* **1998**, *37*, 3874–3876.
[10] G. S. Waldo, S. Yu, J. E. Penner-Hahn, *J. Am. Chem. Soc.* **1992**, *114*, 5869–5870.
[11] S. V. Khangulov, V. V. Barynin, S. V. Antonyuk-Barynina, *Biochim. Biophys. Acta Bioenerg.* **1990**, *1020*, 25–33.
[12] G. S. Waldo, J. E. Penner-Hahn, *Biochemistry* **1995**, *34*, 1507–1512.
[13] M. Shank, V. Barynin, G. Dismukes, *Biochemistry* **1994**, *33*, 15433–15436.
[14] V. L. Pecoraro, M. J. Baldwin, A. Gelasco, *Chem. Rev.* **1994**, *94*, 807–826.
[15] G. C. Dismukes, *Chem. Rev.* **1996**, *96*, 2909–2926.
[16] A. Wu, J. E. Penner-Hahn, V. L. Pecoraro, *Chem. Rev.* **2004**, *104*, 903–938.
[17] A. Gelasco, S. Bensiek, V. L. Pecoraro, *Inorg. Chem.* **1998**, *37*, 3301–3309.
[18] A. E. M. Boelrijk, G. C. Dismukes, *Inorg. Chem.* **2000**, *39*, 3020–3028.
[19] D. Moreno, C. Palopoli, V. Daier, S. Shova, L. Vendier, M. G. Sierra, J. P. Tuchagues, S. Signorella, *Dalton Trans.* **2006**, 5156–5166.
[20] H. Okawa, H. Sakiyama, *Pure Appl. Chem.* **1995**, *67*, 273–280.
[21] H. Sakiyama, H. Okawa, R. Isobe, *J. Chem. Soc. Chem. Commun.* **1993**, 882–884.
[22] L. Dubois, R. Caspar, L. Jacquamet, P.-E. Petit, M.-F. Charlot, C. Baffert, M.-N. Collomb, A. Deronzier, J.-M. Latour, *Inorg. Chem.* **2003**, *42*, 4817–4827.
[23] L. Dubois, D.-F. Xiang, X.-S. Tan, J.-M. Latour, *Eur. J. Inorg. Chem.* **2005**, 1565–1571.
[24] P. Goodson, D. Hodgson, *Inorg. Chem.* **1989**, *28*, 3606–3608.
[25] P. Goodson, D. J. Hodgson, *Inorg. Chim. Acta* **1990**, *172*, 49–57.
[26] P. A. Goodson, A. R. Oki, J. Glerup, D. J. Hodgson, *J. Am. Chem. Soc.* **1990**, *112*, 6248–6254.
[27] N. Kitajima, U. Singh, H. Amagai, M. Osawa, Y. Moro-oka, *J. Am. Chem. Soc.* **1991**, *113*, 7757–7758.
[28] J. Glerup, P. Goodson, A. Hazell, R. Hazell, D. Hodgson, C. McKenzie, K. Michelsen, U. Rychlewska, H. Toftlund, *Inorg. Chem.* **1994**, *33*, 4105–4111.
[29] Y. Gultneh, T. B. Yisgedu, Y. T. Tesema, R. J. Butcher, *Inorg. Chem.* **2003**, *42*, 1857–1867.
[30] Y. Mikata, H. So, A. Yamashita, A. Kawamura, M. Mikuriya, K. Fukui, A. Ichimura, S. Yano, *Dalton Trans.* **2007**, 3330–3334.
[31] S. Mukhopadhyay, S. K. Mandal, S. Bhaduri, W. H. Armstrong, *Chem. Rev.* **2004**, *104*, 3981–4026.
[32] F. Anderegg, *Helv. Chim. Acta* **1967**, *50*, 2330.
[33] D. D. Cox, S. J. Benkovic, L. M. Bloom, F. C. Bradley, M. J. Nelson, L. Que, Jr., D. E. Wallick, *J. Am. Chem. Soc.* **1988**, *110*, 2026–2032.
[34] D. K. Towle, C. A. Botsford, D. J. Hodgson, *Inorg. Chim. Acta* **1988**, *141*, 167–168.
[35] M. Suzuki, H. Senda, Y. Kobayashi, H. Oshio, A. Uehara, *Chem. Lett.* **1988**, 1763–1764.
[36] L. Dubois, L. Jacquamet, J. Pécaut, J.-M. Latour, *Chem. Commun.* **2006**, 4521–4523.
[37] Siemens Analytical X-ray Instruments Inc., Madison, WI, **1995**.
[38] G. M. Sheldrick, University of Göttingen (Germany), **1994**.
[39] G. Blondin, R. Davydov, C. Philouze, M. F. Charlot, S. Styring, B. Akermark, J. J. Girerd, A. Boussac, *J. Chem. Soc. Dalton Trans.* **1997**, 4069–4074.
[40] O. Kahn, *Molecular Magnetism*, VCH, New York, **1993**.

[41] I. Romero, L. Dubois, M. N. Collomb, A. Deronzier, J. M. Latour, J. Pecaut, *Inorg. Chem.* **2002**, *41*, 1795–1806.
[42] K. O. Schäfer, R. Bittl, W. Zweygart, F. Lendzian, G. Haselhorst, T. Weyermüller, K. Wieghardt, W. Lubitz, *J. Am. Chem. Soc.* **1998**, *120*, 13104–13120.
[43] G. Reed, M. Cohn, *J. Biol. Chem.* **1970**, *245*, 662–667.
[44] K. Nakamoto, *Infrared and Raman Spectra of Inorganic and Coordination Compounds*, *Theory and Applications in Inorganic Chemistry*, Wiley-Interscience, **1997**.
[45] H. A. Chu, W. Hillier, N. A. Law, G. T. Babcock, *Biochim. Biophys. Acta Bioenerg.* **2001**, *1503*, 69–82.
[46] A. Cua, J. S. Vrettos, J. C. de Paula, G. W. Brudvig, D. F. Bocian, *J. Biol. Inorg. Chem.* **2003**, *8*, 439–451.
[47] S. Cooper, M. Calvin, *J. Am. Chem. Soc.* **1977**, *99*, 6623–6630.
[48] B. C. Dave, R. S. Czernuszewicz, *Inorg. Chim. Acta* **1994**, *227*, 33–41.
[49] K. Hasegawa, T. A. Ono, *Bull. Chem. Soc. Jpn.* **2006**, *79*, 1025–1031.
[50] M. Suzuki, S. Tokura, M. Suhara, A. Uehara, *Chem. Lett.* **1988**, 477–480.
[51] K. S. Hagen, W. H. Armstrong, H. Hope, *Inorg. Chem.* **1988**, *27*, 967–969.
[52] P. A. Goodson, J. Glerup, D. J. Hodgson, K. Michelsen, E. Pedersen, *Inorg. Chem.* **1990**, *29*, 503–508.
[53] P. Goodson, J. Glerup, D. Hodgson, K. Michelsen, H. Weihe, *Inorg. Chem.* **1991**, *30*, 4909–4914.
[54] D. R. Gamelin, M. L. Kirk, T. L. Stemmler, S. Pal, W. H. Armstrong, J. E. Penner-Hahn, E. I. Solomon, *J. Am. Chem. Soc.* **1994**, *116*, 2392–2399.
[55] Y. Nishida, T. Akamatsu, K. K. Tsuchia, M. Sakamoto, *Polyhedron* **1994**, *13*, 2251–2254.
[56] M. Delroisse, A. Rabion, F. Chardac, D. Tetard, J. B. Verlhac, L. Fraisse, J. L. Seris, *J. Chem. Soc. Chem. Commun.* **1995**, 949–950.
[57] M. Zheng, S. V. Khangulov, G. C. Dismukes, V. V. Barynin, *Inorg. Chem.* **1994**, *33*, 382–387.
[58] L. Dubois, D. F. Xiang, X. S. Tan, J. Pécaut, P. Jones, S. Baudron, L. Le Pape, C. Baffert, S. Chardon-Noblat, M. N. Collomb, A. Deronzier, J. M. Latour, *Inorg. Chem.* **2003**, *42*, 750–760.
[59] R. Tagore, H. Y. Chen, R. H. Crabtree, G. W. Brudvig, *J. Am. Chem. Soc.* **2006**, *128*, 9457–9465.
[60] R. Tagore, R. H. Crabtree, G. W. Brudvig, *Inorg. Chem.* **2007**, *46*, 2193–2203.
[61] C. Costentin, M. Robert, J. M. Saveant, *J. Am. Chem. Soc.* **2006**, *128*, 8726–8727.

Received: August 10, 2007
Published online: February 21, 2008

